Momentum-Topology-Induced Optical Pulling Force

Hang Li,[1] Yongyin Cao,[1] Bojian Shi,[1] Tongtong Zhu,[2] Yong Geng,[3] Rui Feng,[1] Lin Wang,[1] Fangkui Sun,[1] Yuzhi Shi,[4] Mohammad Ali Miri,[5] Manuel Nieto-Vesperinas,[6] Cheng-Wei Qiu,[7,*] and Weiqiang Ding[1,8,†]

[1]*Institute of Advanced Photonics, School of Physics, Harbin Institute of Technology, Harbin 150001, China*
[2]*School of Optoelectronic Engineering and Instrumentation Science, Dalian University of Technology, Dalian 116024, China*
[3]*Center of Ultra-Precision Optoelectronic, Instrument Engineering, Harbin Institute of Technology, Harbin 150001, China*
[4]*School of Electrical and Electronic Engineering, Nanyang Technological University, Singapore 639798, Singapore*
[5]*Department of physics, Queens College of the City University of New York, Queens, New York 11367, USA*
[6]*Instituto de Ciencia de Materiales de Madrid, Consejo Superior de Investigaciones Científicas, Campus de Cantoblanco, Madrid 28049, Spain*
[7]*Department of Electrical and Computer Engineering, National University of Singapore, Singapore 117583, Singapore*
[8]*Collaborative Innovation Center of Extreme Optics, Shanxi University, Taiyuan 030006, Shanxi, China*

(Received 4 August 2019; accepted 30 March 2020; published 10 April 2020)

We report an ingenious mechanism to obtain robust optical pulling force by a single plane wave via engineering the topology of light momentum in the background. The underlying physics is found to be the topological transition of the light momentum from a usual convex shape to a starlike concave shape in the carefully designed background, such as a photonic crystal structure. The principle and results reported here shed insightful concepts concerning optical pulling, and pave the way for a new class of advanced optical manipulation technique, with potential applications of drug delivery and cell sorting.

DOI: 10.1103/PhysRevLett.124.143901

Optical manipulations using various forms of optical force have been widely used in diverse disciplines, including biology [1–6], atom physics [7–10], quantum physics [11–15], and nanotechnology [16–19]. Recently, the counterintuitive optical pulling force (OPF) has attracted broad interest due to its intriguing physics underlying and potential applications [20–26]. An OPF can transport objects towards the source over a long range, rather than pushing them away, which provides a new freedom of optical manipulation beyond trapping and pushing. According to the conservation of linear momentum, the realization of OPF requires the increase of forward momentum of the incident light when scattered by the object, which is the common challenge to be solved in all the mechanisms of OPF generation.

Except for exotic media, such as optically active medium [27–30], chiral medium [31–33], PT symmetry objects [34,35], resonant objects [36,37], and negative refractive index objects [38–40], various structured optical beams are always needed in order to get an OPF, including nonparaxial Bessel beams [21,22,41–43], chiral beams [31–33,44–46], interference fields of multiple beams [47–49], the eigenmodes in a waveguide [50,51] or near an interface [52–54]. The common feature of these engineered fields is their off-axial alignment (relative to the average Poynting vector) of the incident momentum, as shown in Fig. 1(a). When the beam is scattered by an object, the off-axial momentum may be redirected partially or even totally to the incident direction. In this case, the light momentum projection on $+x$ direction increases obviously due to the convex shape of the isofrequency contour, as illustrated in Fig. 1(b), and the OPF is generated according to the linear momentum conservation. Actually, this has been the standard mechanism to get an optical pulling force, which was first proposed by Marston in acoustics more than ten years ago [55,56]. Certainly, we can get an effective OPF using the thermal effect of light on an absorptive object or background [57,58], which is, however, not due to the transfer of light momentum, but due to the Brownian motion.

From Figs. 1(a) and 1(b) and the above discussion, we find that the key factor that prevents the generation of an OPF by a plane wave is the convex-shaped isofrequency contour, which forbids the forward light momentum increase of the plane wave. This is also the reason of structured beams being indispensable in most previous OPF investigations. In order to surmount this restriction, we propose to engineer the intrinsic feature of light momentum in an artificial background, where the isofrequency contour is *concave*, rather than *convex*, as shown in Figs. 1(c) and 1(d).

The change of isofrequency contours in k space from one shape to another is called topological transition in the research of optical metamaterials [59–61]. Since k is proportional to the light momentum p by $p = \hbar k$ [62–65], the shape of isofrequency contour can be named as the topology of light momentum (TLM). In Fig. 1(c), when the incident plane wave is scattered by the object

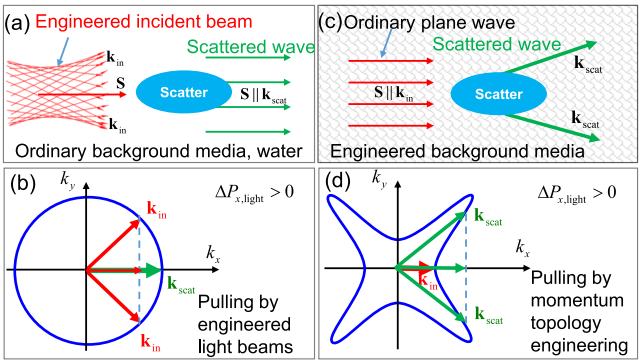

FIG. 1. Illustration of optical pulling force by a plane wave on an ordinary object via engineering the shape of the isofrequency contour, which is named as topology of light momentum (TLM), in the background medium. (a) An engineered light beam with wave vectors ($\mathbf{k}_{\rm in}$) nonparallel to energy flow $\boldsymbol{S}$, such as a Bessel beam, is scattered by an object. After scattering, part of the off-axis momentum may be redirected to the $+x$ direction. Here we show the extreme case of all the momenta being redirected on the $+x$ direction, i.e., $\mathbf{S}\|\mathbf{k}_{\rm scat}$. (b) The forward linear momentum of incident light (red arrows) is increased after scattering by the object (green arrow), thus a pulling force is achieved. (c) Scattering of a single plane wave by an ordinary object in an engineered background. The incident momentum is along the $+x$ direction, and is scattered to off-axis directions by the object. (d) Optical pulling force analysis by the plane wave. The blue curve represents the concave-shaped TLM in the engineered background medium. The forward linear momentum of light is increased, rather than reduced, when it is scattered to off-axis directions by the object. Thus, a negative radiation pressure is exerted on the object.

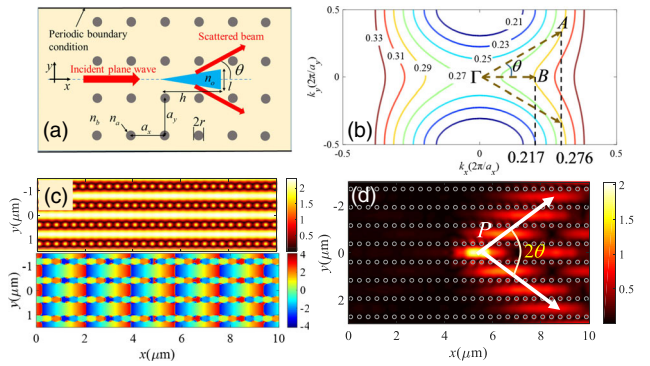

FIG. 2. Light scattering in a concave-shaped TLM environment, which is formed in water by embedding a photonic crystal (PC). (a) Schematic structure of the engineered ambient in water (with a refractive index of $n_b = 1.33$) with silicon rods ($n_a = 3.4$ and radius $r = 0.25\,a_x$) array. The lattice constants along the x and y directions are $a_x = 310$ nm and $a_y = 2.13\ a_x$, respectively. A triangular-shaped object made of Al_2O_3 ($n_o = 1.75$), base length $l = 0.2\ \mu$m, and height $h = 1\ \mu$m is set between two neighboring rows. A plane wave is launched from the left-handed side. (b) TLM in the background medium for TE polarization, (electric vector along the z direction). In the normalized frequency: (0.27~0.33) $(2\pi c/a_x)$, the concave-shaped TLM is available. When the light is scattered from the axial direction ΓB to an off-axial direction ΓA, the wave vector will increase from $0.217(2\pi/a_x)$ to $0.276(2\pi/a_x)$. (c) Distribution of electric field amplitude (upper part) and phase (lower part) of the incident field of E_z in the PC. The incident frequency is $0.29(2\pi c/a_x)$. (d) Distribution of $|E_z|$ of scattered field by the triangular object located at $x = 5$ and $y = 0\ \mu$m. The white arrows indicate the directions of the Poynting vectors ($\pm 40°$). The small gray circles represent the photonic crystal lattice.

from axial to off-axial directions, the projection of the light momentum on the $+x$ direction will increase obviously (rather than decrease) due to the concave-shaped TLM, as illustrated in Fig. 1(d). As a result, the object will experience an OPF according to the linear momentum conservation.

This mechanism focuses on the engineering of the TLM of the background medium, but not the incident light beam. Thus, it can be regarded as the *complementary* mechanism comparing to the widely used mechanism adopting structured light beams. From this point of view, our proposal is conceptually significant, and valuable for further understanding of optical pulling force and the light momentum in medium [62,66]. For these reasons, we except this work will stimulate further research, and open new possibilities for advanced optical manipulation techniques.

In order to get a medium with the concave-shaped TLM, photonic crystal (PC) is the best candidate according to its powerful capacity demonstrated in band engineering [67–70]. Physically, the relations between the TLM and the parameters of the PC are complicated. However, the following principles are helpful in the design of the PC. (I) Since the concave-shaped EFC means highly anisotropic, a modified square lattice (i.e., rectangular lattice) with $a_x \neq a_y$ should be selected, because it has a lower rotational symmetry (C2 symmetry) than the triangular and square lattices (C6 and C4, respectively). (II) Selecting the source frequency in the second band of the PC, because the PC behaviors like an isotropic medium for the low frequencies in the first band (effective medium approximation). (III) Using a numerical method to check the TLM and tune the structural parameters finely (the lattice constants and/or the radius of the atoms) to get an optimized PC matching the target source frequency.

The designed rectangular PC for the target wavelength ($\lambda_0 = 1064$ nm is used as an example) is shown in Fig. 2(a) The lattice constants are $a_x = 310$ nm and $a_y = 2.13\,a_x$. The radius and refractive index of the silicon rods are $r = 0.25\,a_x$ and $n = 3.4$, respectively. The whole structure is immersed in water ($n_b = 1.33$). Figure 2(b) shows the TLM of the second band of TE polarization (with electric vector along the z direction), which is calculated by using the plane wave expansion method [71]. Clearly, the TLM is concave in a wide frequency range from $0.21(2\pi c/a_x)$ to $0.33(2\pi c/a_x)$, and for the OPF along the x direction, the frequency between $0.27(2\pi c/a_x)$ and $0.33(2\pi c/a_x)$ should be selected.

A plane wave, TE polarized, with normalized frequency $\omega = 0.29\ (2\pi c/a_x)$ is launched into the structure from the left-handed side, which corresponds to the target wavelength of 1064 nm (in vacuum). Fig. 2(c) shows the electric field amplitude (upper part), and phase distributions (lower part), and a plane wave front can be observed clearly. Here, the finite difference in the time-domain (FDTD) algorithm is used in simulation. Periodic boundary condition, and perfectly matched layers (PML) are set in the x and y directions, respectively [72], which ensures the incident light momentum being along the $+x$ direction.

A triangle-shaped dielectric object with its base length $l = 0.2\ \mu$m, height $h = 1\ \mu$m, and refractive index of $n_o = 1.75$ (such as Al_2O_3) is set along the symmetry axis $y = 0$, as shown in Fig. 2(a). The triangular shape is selected because, according to the viewpoint of geometrical optics, it can reflect the incident plane wave to off-axial directions without backscattering. Although the geometrical method is not rigorous in the present situation, it can yield a rather good approximation as shown in Fig. 2(d), which depicts the mode pattern $|E_z|$ of the scattered field (the incident field is excluded from the total field) by the triangular particle. One can observe that the incident field is symmetrically scattered into two main directions without obvious backscattering. According to the analysis above, the momentum of light along the $+x$ direction will increase, and the object should experience an OPF.

We quantitatively evaluate the optical pulling force using the linear momentum conservation law (LMCL), as shown in Fig. 3(a) by the dotted (red) curve. Suppose $N(\theta)$ photons are scattered to the direction of θ from the incident direction of $\theta = 0$, then the x component of the momentum imparted to the object is

$$\Delta P_x = N_{\text{in}}\hbar k_0 - \int \hbar k_x(\theta) N(\theta) d\theta, \tag{1}$$

where $\hbar$ is the reduced Plank constant, and k_0 is the wave vector of the incident wave. $k_x(\theta)$ is the x component of the wave vector in the θ direction. For an incident power P, the number of photons incident on the object in Δt is $N_{\text{in}} = P\Delta t/(\hbar\omega)$. Suppose the scattering probability at angle θ is $S(\theta)$, then the number of photons scattered in the θ direction is $N(\theta) = N_{\text{in}} S(\theta)$. Therefore, the total optical force F_x exerted on the object is

$$F_x = \frac{\Delta P_x}{\Delta t} = \frac{P[N_{\text{in}}\hbar k_0 - \int \hbar k_x(\theta) N(\theta) d\theta]}{N_{\text{in}}\hbar\omega} = \frac{P}{\omega}[k_0 - \int k_x(\theta) S(\theta) d\theta]. \tag{2}$$

According to the scattered field distribution in Fig. 2(d), the incident light is mainly scattered into $\pm 40°$, while the scattering to other directions (including the reflection), can be neglected in the first order approximation. According to Fig. 2(b), the wave vectors along incident direction $\theta = 0°$, and scattering direction of $\pm 40°$ are $0.217(2\pi/a_x)$ and $0.276(2\pi/a_x)$, respectively. Substituting these values in Eq. (2), a pulling force of about -0.9 pN/mW is obtained (see Sec. I in the Supplemental Material [73] for more calculation details), as shown by the dotted line (in red) in Fig. 3(a). In Eq. (2), we have assumed that the pulling force is mainly acted on the object, but not on the nanorods of the background lattice (see Sec. II in Supplemental Material [73] for more details).

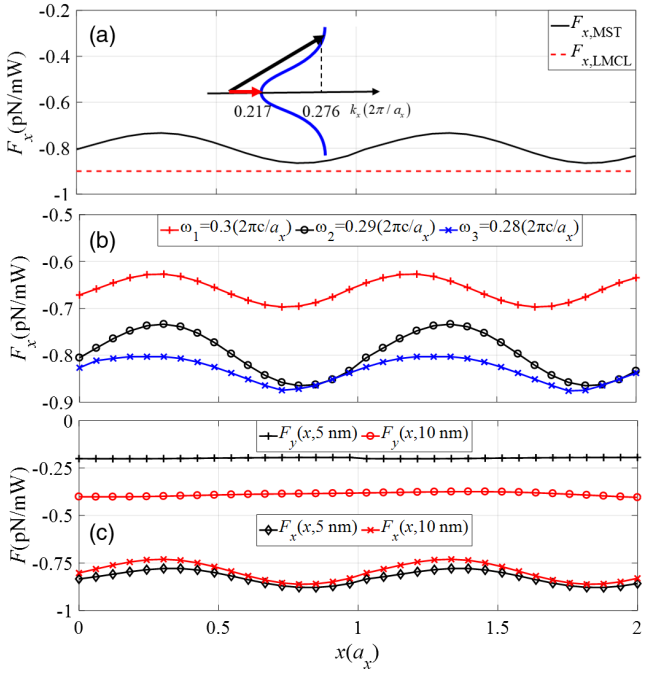

FIG. 3. Optical forces exerted on the object defined in Fig. 2. (a) $F_x(x, 0)$ on the object. The dashed line (in red color) shows the force directly calculated from the linear momentum conservation law [see Eq. (2)]. The inset shows the wave vectors of the incident field ($\theta = 0°$) and scattered field ($\theta = 40°$). The solid curve (in black) corresponds to the pulling forces obtained by integration of Maxwell's stress tensor [see Eq. (3)]. (b) Wideband feature of the optical pulling force at three different normalized frequencies (in unit of $2\pi c/a_x$) of $\omega_1 = 0.30$, $\omega_2 = 0.29$, and $\omega_3 = 0.28$. (c) Transverse stability of the optical pulling force when the object is at off-axis positions. $F_y(y)$ is always a restoring force, and $F_x(x)$ is always a pulling one when the object is at off-axis positions of $y = 5$ and 10 nm.

The OPF calculated from Eq. (2) agrees very well with the numerical results obtained by integration of the Maxwell stress tensor (MST) on a closed path L surrounding the object [74], i.e., $\langle \mathbf{F}_{\text{total}} \rangle = \oint_L \langle \mathbf{T} \rangle \cdot dl$ where

$$\langle \mathbf{T} \rangle = \frac{1}{2}\text{Re}[\mathbf{D} \otimes \mathbf{E}^* + \mathbf{H} \otimes \mathbf{B}^* - \frac{1}{2}\overleftrightarrow{\mathbf{I}}(\mathbf{E} \cdot \mathbf{D}^* + \mathbf{H} \cdot \mathbf{B}^*)]. \tag{3}$$

Here, $\langle \cdot \rangle$ means time average, $\otimes$ stands for dyadic operation, and $\overleftrightarrow{\mathbf{I}}$ is the unit tensor. The resulting OPF

are shown by the solid curve (in black color) in Fig. 3(a), where the object moves from $x = 0$ to $x = 3a_x$. Clearly, the optical force along the x direction is always negative, which means the object will be continuously pulled by the incident wave.

Although there is more than one light momentum formula that can be selected in optical force calculation, the Minkowski momentum (rather than the Abraham momentum) has been used for the following reasons. (i) It has been revealed that the Minkowski momentum is carried by the combined system of light and matter, while the Abraham momentum is carried by the light wave only [62]. It has been theoretically verified that the momentum associated with the matter also contributes to the optical force on an immersed (and semi-immersed) object [75]. Second, in several other similar experimental configurations, such as the interfacial tractor beam [52], and radiation pressure on mirrors immersed in liquids [76,77], the application of Minkowski momentum has been experimentally justified. According to these two reasons, the Minkowski momentum is used here in order to get the optical forces consistent with experimental observations.

The OPF also has several other merits of stable, broadband, and robust to the parameters, which are extremely desirable in experiment. In Fig. 3(b), the OPF for different incident frequencies (in units of $2\pi c/a_x$) of $\omega_1 = 0.30$, $\omega_2 = 0.29$, and $\omega_3 = 0.28$, are shown by the red, black, and blue curves, respectively. Clearly, OPFs are achieved for all the three frequencies. More importantly, the force amplitude at $\omega_3 = 0.28$ is the largest, while that at $\omega_1 = 0.30$ is the smallest, which agree well with the shape of the isofrequency contours in Fig. 2(b). In addition, the operation frequency can be easily scaled to the other band by tuning the lattice constant. For example, when $a_x = 450$ nm, the wavelength will shift to 1550 nm for $\omega = 0.29$. This wide-band feature is very useful in experiments, which also makes the OPF robust to material dispersion (see Sec. III in Supplemental Material [73] for more details).

Figure 3(c) shows the transverse stability of this pulling manipulation. When the object is shifted along the y direction to $y_1 = 5$ and $y_2 = 10$ nm, the forces $F_y(x, y_{1,2})$ are shown by the black ($y_1 = 5$ nm) and red ($y_2 = 10$ nm) lines, respectively. Clearly, F_y is a restoring force driving the object to the equilibrium position of $y = 0$. Actually, F_y is an intensity gradient force pointing to the middle line of two neighboring rows of rods [78], which can be observed in Fig. 2(a).

Although we have used a triangular-shaped object in the above analysis to reduce the harmful backscattering, the OPF is not sensitive to the shape and refractive index of the object. In Fig. 4(a), we present $\max[F_x(x, 0)]$ on an elliptical object with semiaxes r_x and r_y. The refractive index n_o varies from 1.4 to 2.6, and r_x changes from 0.1 to 1 μm ($r_y = 0.1$ μm is fixed for convenience). In most regions in the parametric space (n_o, r_x), the optical force is

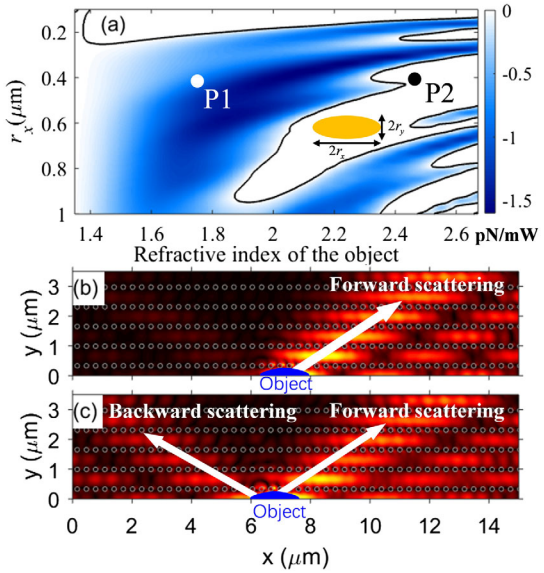

FIG. 4. (a) Changes of $\max[F_x(x, 0)]$ exerted on different elliptical objects (see the inset). The refractive index varies from 1.4 to 2.6, and the semiaxis r_x changes from 0.1 to 1 μm, ($r_y = 0.1$ μm is fixed for convenience). In the colored region, the objects experience continuous pulling forces when they shift along x axis. P1 and P2 are two representative objects analyzed in detail in (b) and (c). (b) Scattered field by the object P1. Because of the symmetry of the structure, only the half space of $y > 0$ is shown. Forward scattering occurs which generates a continuous pulling force. (c) Scattered field by the object P2. Backward scattering results in a pushing force and cancels the pulling force generated by the forward scattering.

pulling. Figures 4(b) and 4(c), respectively, show the scattered fields for the objects of P1 and P2 marked in Fig. 4(a), where only the half spaces of $y > 0$ are shown due to the symmetry. The absence of pulling force at P2 can be attributed to the harmful backscattering of the object, which generates a pushing force larger (in amplitude) than the pulling force.

In this new mechanism, OPF by a single plane wave becomes ubiquitous in a medium with concave-shaped TLM, which makes the forward momentum increase easy and efficient, just like the optical pushing force in an ordinary medium (with a convex-shaped TLM). This mechanism not only provides a new avenue for OPF generation, also greatly contributes to the further understanding of light momentum in medium. The potential applications of this new result include particle sorting, drug deliverance, and even diseased cell diagnosis (see Sec. IV in Supplemental Material [73] for more details).

In conclusion, we have uncovered a novel mechanism to achieve optical pulling forces by tailoring the topology of light momentum (TLM) in a designed background. When the TLM is a starlike concave shape, rather than the convex shape in ordinary medium, the light momentum scattered by the object to off-axis directions will be larger than the

incident momentum. As a result, the forward momentum of the incident plane wave increases, and an optical pulling force is obtained. In a rectangular lattice photonic crystal made of silicon rods in water, we theoretically and numerically demonstrated the transversely stable, long range, object insensitive, and wide-band optical pulling force. We expect the mechanism and results reported here will open a new avenue in the field of optical manipulation technology and in its development, also playing a relevant role in related areas.

This work was supported by National Natural Science Foundation of China (Grants No. 11874134 and No. 11704088). We thank the HPC Studio at Physics Department of Harbin Institute of Technology for access to computing resources through INSPUR-HPC@PHY.HIT. C-W.Q acknowledges the support from the Ministry of Education, Singapore (Grant No. R-263-000-D11-114). M. N-V. acknowledges support from Ministerio de Ciencia, Innovacion y Universidades of Spain through Grants No. FIS2014-55563-REDC, No. FIS2015-69295-C3-1-P, and No. PGC2018-095777-B-C21.

*Corresponding author.
chengwei.qiu@nus.edu.sg
†Corresponding author.
wqding@hit.edu.cn

[1] A. Ashkin and J. M. Dziedzic, Science **235**, 1517 (1987).
[2] A. Ashkin, J. M. Dziedzic, and T. Yamane, Nature (London) **330**, 769 (1987).
[3] J. T. Finer, R. M. Simmons, and J. A. Spudich, Nature (London) **368**, 113 (1994).
[4] C. L. Asbury, A. N. Fehr, and S. M. Block, Science **302**, 2130 (2003).
[5] F. M. Fazal and S. M. Block, Nat. Photonics **5**, 318 (2011).
[6] K. O. Greulich, Rep. Prog. Phys. **80**, 026601 (2017).
[7] L. R. Liu, J. D. Hood, Y. Yu, J. T. Zhang, N. R. Hutzler, T. Rosenband, and K.-K. Ni, Science **360**, 900 (2018).
[8] T. K. Langin, G. M. Gorman, and T. C. Killian, Science **363**, 61 (2019).
[9] B. He, L. Yang, Q. Lin, and M. Xiao, Phys. Rev. Lett. **118**, 233604 (2017).
[10] M. Hosseini, Y. Duan, K. M. Beck, Y. T. Chen, and V. Vuletic, Phys. Rev. Lett. **118**, 183601 (2017).
[11] M. Aspelmeyer, T. J. Kippenberg, and F. Marquardt, Rev. Mod. Phys. **86**, 1391 (2014).
[12] D. Malz, L. D. Toth, N. R. Bernier, A. K. Feofanov, T. J. Kippenberg, and A. Nunnenkamp, Phys. Rev. Lett. **120**, 023601 (2018).
[13] K. E. Khosla, M. R. Vanner, N. Ares, and E. A. Laird, Phys. Rev. X **8**, 021052 (2018).
[14] H. Zoubi and K. Hammerer, Phys. Rev. Lett. **119**, 123602 (2017).
[15] C. H. Metzger, Nature (London) **432**, 1002 (2004).
[16] O. M. Wani, H. Zeng, and A. Priimagi, Nat. Commun. **8**, 15546 (2017).
[17] Y. Xiao, S. Zarghami, K. Wagner, P. Wagner, K. C. Gordon, L. Florea, D. Diamond, and D. L. Officer, Adv. Mater. **30**, 1801821 (2018).
[18] D. E. Smalley *et al.*, Nature (London) **553**, 486 (2018).
[19] D. Gao, W. Ding, M. Nieto-Vesperinas, X. Ding, M. Rahman, T. Zhang, C. T. Lim, and C.-W. Qiu, Light Sci. Appl. **6**, e17039 (2017).
[20] S. Sukhov and A. Dogariu, Opt. Lett. **35**, 3847 (2010).
[21] J. Chen, J. Ng, Z. Lin, and C. T. Chan, Nat. Photonics **5**, 531 (2011).
[22] A. Novitsky, C.-W. Qiu, and H. Wang, Phys. Rev. Lett. **107**, 203601 (2011).
[23] J. J. Sáenz, Nat. Photonics **5**, 514 (2011).
[24] W. Ding, T. Zhu, L.-M. Zhou, and C.-W. Qiu, Adv. Photonics **1**, 024001 (2019).
[25] A. Dogariu, S. Sukhov, and J. J. Sáenz, Nat. Photonics **7**, 24 (2013).
[26] S. Sukhov and A. Dogariu, Rep. Prog. Phys. **80**, 112001 (2017).
[27] A. Mizrahi and Y. Fainman, Opt. Lett. **35**, 3405 (2010).
[28] K. J. Webb and Shivanand, Phys. Rev. E **84**, 057602 (2011).
[29] G. Li, M. Wang, H. Li, M. Yu, Y. Dong, and J. Xu, Opt. Mater. Express **6**, 388 (2016).
[30] X. Bian, D. L. Gao, and L. Gao, Opt. Express **25**, 24566 (2017).
[31] K. Ding, J. Ng, L. Zhou, and C. T. Chan, Phys. Rev. A **89**, 063825 (2014).
[32] D. E. Fernandes and M. G. Silveirinha, Phys. Rev. A **91**, 061801(R) (2015).
[33] D. E. Fernandes and M. G. Silveirinha, Phys. Rev. Applied **6**, 014016 (2016).
[34] R. Alaee, J. Christensen, and M. Kadic, Phys. Rev. Applied **9**, 014007 (2018).
[35] R. Alaee, B. Gurlek, J. Christensen, and M. Kadic, Phys. Rev. B **97**, 195420 (2018).
[36] H. Chen, S. Liu, J. Zi, and Z. Lin, ACS Nano **9**, 1926 (2015).
[37] Y. J. L. Chu, E. M. Jansson, and G. A. Swartzlander, Phys. Rev. Lett. **121**, 063903 (2018).
[38] A. Salandrino and D. N. Christodoulides, Opt. Lett. **36**, 3103 (2011).
[39] J. Nemirovsky, M. C. Rechtsman, and M. Segev, Opt. Express **20**, 8907 (2012).
[40] A. V. Maslov, Phys. Rev. Lett. **112**, 113903 (2014).
[41] L. Zhang and P. L. Marston, Phys. Rev. E **84**, 035601(R) (2011).
[42] A. Novitsky, C.-W. Qiu, and A. Lavrinenko, Phys. Rev. Lett. **109**, 023902 (2012).
[43] N. Wang, J. Chen, S. Liu, and Z. Lin, Phys. Rev. A **87**, 063812 (2013).
[44] S.-H. Lee, Y. Roichman, and D. G. Grier, Opt. Express **18**, 6988 (2010).
[45] L. Carretero, P. Acebal, C. Garcia, and S. Blaya, Opt. Express **23**, 20529 (2015).
[46] B. Hadad, S. Froim, H. Nagar, T. Admon, Y. Eliezer, Y. Roichman, and A. Bahabad, Optica **5**, 551 (2018).
[47] S. Sukhov and A. Dogariu, Phys. Rev. Lett. **107**, 203602 (2011).

[48] O. Brzobohatý, V. Karásek, M. Šiler, L. Chvátal, T. Čižmár, and P. Zemánek, Nat. Photonics **7**, 123 (2013).
[49] D. B. Ruffner and D. G. Grier, Phys. Rev. Lett. **109**, 163903 (2012).
[50] V. Intaraprasonk and S. Fan, Opt. Lett. **38**, 3264 (2013).
[51] T. Zhu, A. Novitsky, Y. Cao, M. R. C. Mahdy, L. Wang, F. Sun, Z. Jiang, and W. Ding, Appl. Phys. Lett. **111**, 061105 (2017).
[52] V. Kajorndejnukul, W. Ding, S. Sukhov, C.-W. Qiu, and A. Dogariu, Nat. Photonics **7**, 787 (2013).
[53] M. I. Petrov, S. V. Sukhov, A. A. Bogdanov, A. S. Shalin, and A. Dogariu, Laser Photonics Rev. **10**, 116 (2016).
[54] A. Ivinskaya, N. Kostina, A. Proskurin, M. I. Petrov, A. A. Bogdanov, S. Sukhov, A. V. Krasavin, A. Karabchevsky, A. S. Shalin, and P. Ginzburg, ACS Photonics **5**, 4371 (2018).
[55] P. L. Marston, J. Acoust. Soc. Am. **120**, 3518 (2006).
[56] P. L. Marston, J. Acoust. Soc. Am. **122**, 3162 (2007).
[57] V. Shvedov, A. R. Davoyan, C. Hnatovsky, N. Engheta, and W. Krolikowski, Nat. Photonics **8**, 846 (2014).
[58] J. Lu, H. Yang, L. Zhou, Y. Yang, S. Luo, Q. Li, and M. Qiu, Phys. Rev. Lett. **118**, 043601 (2017).
[59] A. V. Shchelokova, D. S. Filonov, P. V. Kapitanova, and P. A. Belov, Phys. Rev. B **90**, 115155 (2014).
[60] H. N. S. Krishnamoorthy, Z. Jacob, E. Narimanov, I. Kretzschmar, and V. M. Menon, Science **336**, 205 (2012).
[61] J. S. Gomez-Diaz, M. Tymchenko, and A. Alù, Phys. Rev. Lett. **114**, 233901 (2015).
[62] P. W. Milonni and R. W. Boyd, Adv. Opt. Photonics **2**, 519 (2010).
[63] M. Buchanan, Nat. Phys. **3**, 73 (2007).
[64] R. Loudon, S. M. Barnett, and C. Baxter, Phys. Rev. A **71**, 063802 (2005).
[65] G. K. Campbell, A. E. Leanhardt, J. Mun, M. Boyd, E. W. Streed, W. Ketterle, and D. E. Pritchard, Phys. Rev. Lett. **94**, 170403 (2005).
[66] B. A. Kemp, Nat. Photonics **10**, 291 (2016).
[67] S. John, Phys. Rev. Lett. **58**, 2486 (1987).
[68] E. Yablonovitch, Phys. Rev. Lett. **58**, 2059 (1987).
[69] H. Watanabe and L. Lu, Phys. Rev. Lett. **121**, 263903 (2018).
[70] T. Zhu *et al.*, Phys. Rev. Lett. **120**, 123901 (2018).
[71] S. G. Johnson and J. D. Joannopoulos, Opt. Express **8**, 173 (2001).
[72] S. D. Gedney, IEEE Trans. Antennas Propag. **44**, 1630 (1996).
[73] See Supplemental Material at http://link.aps.org/supplemental/10.1103/PhysRevLett.124.143901 for the OPF obtained using linear momentum conservation, the zero force on the background lattice, the effect of material dispersion on the wide band feature of the OPF, and a potential application of this work.
[74] R. N. C. Pfeifer, T. A. Nieminen, N. R. Heckenberg, and H. Rubinsztein-Dunlop, Rev. Mod. Phys. **79**, 1197 (2007).
[75] C.-W. Qiu, W. Ding, M. R. C. Mahdy, D. Gao, T. Zhang, F. C. Cheong, A. Dogariu, Z. Wang, and C. T. Lim, Light Sci. Appl. **4**, e278 (2015).
[76] R. Jones and J. Richards, Proc. R. Soc. A **221**, 480 (1954).
[77] R. Jones and B. Leslie, Proc. R. Soc. A **360**, 347 (1978), https://www.jstor.org/stable/79586?seq=1.
[78] A. Ashkin, J. M. Dziedzic, J. E. Bjorkholm, and S. Chu, Opt. Lett. **11**, 288 (1986).